Distinguishing between mechanical and electrostatic interaction in single pass multi frequency Electrostatic Force Microscopy measurements on a molecular material

Marta Riba-Moliner,[†] *Narcis Avarvari,*[‡] *David. B. Amabilino,* [§] *Arántzazu González-Campo,*[†] *Andrés Gómez-Rodríguez*[*,†]

[†] Institut de Ciència de Materials de Barcelona (ICMAB-CSIC), Campus UAB, 08913 Bellaterra, Barcelona, Spain

[‡] Laboratoire MOLTECH-Anjou UMR 6200, UFR Sciences, CNRS, Université d'Angers, Bât. K, 2 Bd. Lavoisier, 49045 Angers, France

[§] School of Chemistry, The University of Nottingham, University Park, Nottingham NG72RD United Kingdom

KEYWORDS Electrostatic Force Microscopy (EFM), crosstalk, artifacts, Bimodal Atomic Force Microscopy, Multifrequency Atomic Force Microscopy

ABSTRACT

Single-pass Electrostatic Force Microscopy is postulated as one of the most advanced techniques in terms of spatial resolution and fastness in data acquisition for the study of electrostatic phenomena at the nanoscale. However, crosstalk anomalies, in which mechanical interactions combine with tip-sample electrostatic forces, are still a major issue to overcome, specifically in soft and biological samples. In this paper we propose a novel method based on Bimodal-Atomic Force Microscopy to distinguish mechanical crosstalk from electrostatic images. The method is based in the comparison of Bimodal AFM images with electrostatic ones, where pure mechanical interaction can be discerned from a mixture of mechanical and electrostatic interactions. The proposed method is optimized and demonstrated using a supramolecular charge transfer material. Finally, the method is used as a tool to depict different crosstalk levels in organic samples, discerning between electrical and mechanical interactions. This kind of observation is important for obtaining accurate descriptions of charge distribution in samples made from organic and molecular layers and materials.

INTRODUCTION

Electrostatic Force Microscopy (EFM) and Kelvin Probe Force Microscopy (KPFM) techniques have become widely and commonly used in surface characterization of organic semiconducting thin films because they are considered easy and non-destructive tools.[1–5] Concretely, EFM provides the feasibility of studying electrostatic properties - such as dielectric permittivity of insulating materials, surface charge distribution, oxidation and reduction processes - as well as allowing the distinction between conducting and insulating areas in hybrid materials.[6–12] The

EFM technique can be implemented using two different set-ups: dual-pass and single-pass modes.[13]

In the dual-pass EFM mode, a metallic tip is used to scan the surface acquiring the topography in the first pass.[13] Sequentially, the sample is re-scanned biasing the tip with an AC and a DC voltage, to collect amplitude and phase variations due to tip-sample electrostatic interactions. Because the electrostatic interaction depends strongly on the tip-sample distance, the Z-piezo of the equipment is fed with the topographic signal during the second pass, keeping the tip-sample distance as constant as possible. Dual-pass provides an accurate way to quantify electrostatic interactions. However, main drawbacks are the increased acquisition time (compared with single pass), the absolute necessity to reduce drift (especially in the Z-axis), and consequently, diminishing the lateral resolution of electrostatic response from the acquired signal. .

Single-pass EFM has been proposed as a solution to overcome the difficulties of the dual-pass mode.[14] In the single-pass setup, a metallic tip is used to obtain topography using dynamic mode, while, at the same time, an AC and a DC voltage is applied to the tip. This approach is a faster method for data acquisition with respect to dual-pass EFM, with increased lateral[13]. The AC tip voltage frequency is a key-factor to improve the signal-to-noise ratio and to decrease the topography crosstalk into the electrostatic signal. Choosing the second resonance frequency of the cantilever is, in terms of signal quality, the most appropiate.[15] With in the second resonance mode, the second resonance mode Q factor increases, allowing measurements of forces in the order of magnitude of pN.[16,17] However, the use of this second resonance mode may induce crosstalk and resulting sample artifacts, where the tip vibration is not due to electrostatic phenomena. While using this mode, the electrostatic interactions cause the tip vibrating at the second resonance frequency.

Bimodal AFM is an advanced characterization mode where the AFM cantilever is exited at its first and second resonance frequency.[18] The first resonant frequency is used to depict sample topography, while its second resonance frequency is used to provide the mechanical properties of the specimen.[18,17] In our case, we have interpreted EFM mode, using the second resonance as doing an electrostatic driven Bimodal AFM, where electrostatic interactions drive the cantilever at its second resonance mode, mixing mechanical properties and electrostatic interactions. Hence, the crosstalk phenomena is inherent to the measurement process, where its minimization is an ongoing challenge of great interest for the scientific community.[19–21]

In this paper we describe a novel method based on Bimodal AFM with the aim to glean accurate and "clean" electrostatic information separated from mechanical artifacts in EFM images. For this reason, we made use of the second resonance mode of the cantilever, i.e. Dual Resonance Electrostatic Force Microscopy (DREFM). Our approach revealed a decrease of the crosstalk phenomenon with respect to regular EFM measurements. The study presented here is divided into two main subsections: the first corresponding to the setup of the equipment and the confirmation that cantilever dynamics in Bimodal and EFM modes can be compared, and the second to experimental tests using a doped organic sample, with charge transportation properties, as a soft material to challenge the validity of the proposed methodology.

SETUP

The setup of the equipment for the DREFM approach is shown in **Fig. 1a** in which an AC voltage signal drive is connected to cantilever piezo with a frequency that matches the first resonance frequency of the cantilever (ω_1). The amplitude (A_1) is used to depict the topography

through the use of a constant amplitude feedback. A second AC voltage is directly rooted to the tip; meanwhile a DC voltage is added to the AC voltage. The use of the DC voltage is to increase the tip-sample electrostatic interactions due to an increased tip-sample surface potential difference.[22,23] The frequency of this second AC voltage is set to match the second resonance mode of the cantilever (ω_2) so that changes in the amplitude (A_2) provide information of the electrostatic properties. In the setup for the bimodal mode (**Fig. 1b**), two AC voltage generators are connected to the cantilever piezo, which imposes the vibration of the cantilever at the frequencies ω_1 and ω_2, the first and second resonant modes of the cantilever.[24–26] Therefore, the first mode of resonance, with amplitude A_1, is used to reveal the topography using a constant amplitude feedback and the second mode. On the other hand, with amplitude A_2, information of dissimilar mechanical properties of the surface can be provided. Following the objective of obtaining a clear interaction tip-surface, we employed the second eigenmode for nanomechanical mapping in order to exploit its higher Q-factor compared to the first eigenmode.

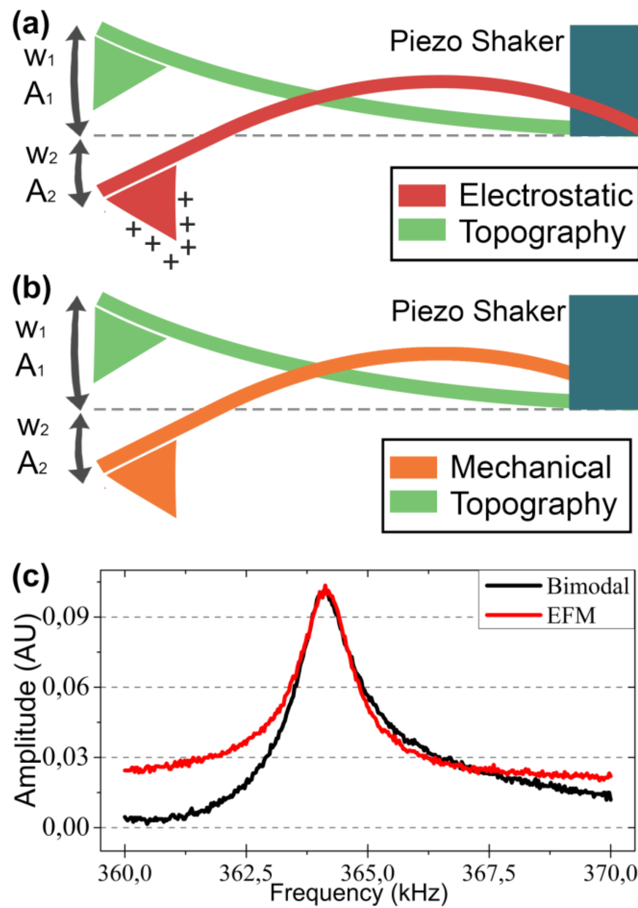

Fig. 1 a) and b) Representations of the vibrational movements of electrostatically-driven and piezo-shaker-driven cantilever. c) Frequency sweeps of the cantilever acquired in EFM and bimodal modes.

In order to demonstrate that the cantilever dynamics in bimodal and EFM are comparable, the study of a electrostatic driven cantilever were conducted. Sumali and Epp already demonstrated that an electrostatically-driven cantilever can be equivalent to a piezo-shaker-driven cantilever, the cantilever movement being independent of the position (at the base or at the edge of the cantilever) of the driving force applied.[27] By solving classical mechanical equations, the authors conclude that both piezo-driven cantilever and electrostatic driven cantilever dynamics are

equivalent. Moreover, the equivalent base acceleration for a cantilever driven by electrostatic force, follows the above equation (**1**): [27]

$$-\ddot{e}_{\square} = \frac{\square_{1}}{(\square_{\square} - \square_{0})^{\square_{3}}} - \frac{\square_{1}}{(-\square_{0})^{\square_{3}}} \quad \mathbf{(1)}$$

where $\ddot{e}_{\square}$ is the equivalent base acceleration of the cantilever, $\square_{\square}$ is the relative tip deflection and $\square_{0}, \square_{1}, \square_{3}$ are numerical parameters that depends into the specific size and Young's modulus of the cantilever used. This approach was evaluated correlating the resonance frequency and Q-factor of an electrostatically-driven and piezo-shaker-driven cantilever (**Fig. 1c**). All the data were obtained after performing two consecutive frequency sweeps, in bimodal and in EFM modes, without changing the cantilever and at a fixed tip-sample distance and laser position. The Q-factor values and the resonance frequency were calculated using the theory of standard resonators, which were found to be 352.9 and 364.1 kHz for EFM and 343.4 and 364.2 kHz for bimodal measurement modes, respectively.[28,29] The fact that the Q-factor values and the resonance frequency are extremely similar for both cases validates the theoretical approach, and, consequently, images resulting from electrostatically- and piezo-shaker driven cantilevers can be compared. As a result of that, bimodal images, which provide mechanical information of samples, can be used to compare with EFM images, which provide electrostatic information with crosstalk mechanical properties.

Another important factor to take into account when comparing bimodal and EFM signals is the free amplitude and set-point values used in order to obtain the topography signal. The quantification of the amplitude was achieved by plotting a curve of the amplitude *versus* distance (see **Fig. S1** and **Fig. S2 in Supplementary Information**).[30] Not only is the free amplitude important but also the set-point, which is associated with the force applied to the sample. For this

reason, a standard value of 40-60 nm for the amplitude recorded at ω_1, together with a free amplitude reduction of 25-35% were the parameters used for fixing the set-point value (these values strongly depend on the specific sample).[18] The amplitude of the second mode ranged between 0.2-1.0 nm, depending on the specific tip-sample electrostatic interaction for such material It is important to note that the final amplitude values displayed here were given in volts (V), instead of distance units, which were extracted from the setup measurements shown above, to facilitate the comparison of the results . The aforementioned parameters used are in accordance with previous work reported by Stark *et al.*, where the reduction of the crosstalk between topography and electrostatic signals was studied.[23]

MEASUREMENT OF A DOPED ORGANIC MATERIAL

The objective with the proposed setup was to discern the electrostatic from mechanical contribution of organic samples by the use of an electrostatically-driven cantilever. Usually, as the force exerted by the cantilever depends on the electrostatic properties of the sample and, at the same time, the cantilever movement can be dependent on the different mechanical properties, the electrostatic outgoing signal can mislead the interpretation of results. For this reason, a doped organic sample with electrostatic response was chosen, based on the C_3-symmetric enantiopure tris(TTF) (*N,N',N''*-tris[3[3'-bis[(*S*)-2-methylbutylthio]-tetrathiafulvalenyl]-formylamino]-2,2'-bipyridyl]–benzene-1,3,5,-tricarboxamide) (C_3-TTF) **(Fig. 2).**

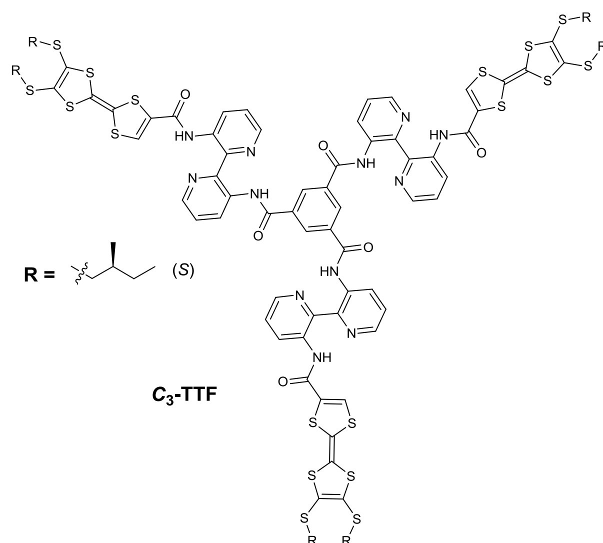

Fig. 2 C_3-TTF molecule used for this study.

This electroactive precursor has already been shown to self-assemble by π-π stacking and TTF···TTF interactions to give, depending on the conditions, right-handed coiled superhelices[31] or microcroissants[32] by precipitation in dioxane. The sense of helicity changes from solution to the solid state and is imposed by the enantiopure peripheral chains. Indeed, an odd-even effect has been observed in another series of compounds with citronellyl and dihydro-citronellyl substituents.[33] Furthermore, tetrathiafulvalenes (TTFs) are excellent π-electron donor units that are widely studied in molecular electronic applications due to their *p*-type character and stable doped states.[3429] As electron-donor species, TTFs can be oxidized reversibly under exposure to an appropriate oxidant. Three oxidization states are present in TTFs, the neutral TTF (TTF^0), that exists under ambient conditions, the cation-radical ($TTF^{+\bullet}$) and the dication (TTF^{2+}) and these three states can be accessed and controlled sequentially through one electron processes, such as doping or de-doping. Accordingly, it has been shown that iodine doping of achiral derivative with ethyl substituents instead of 2-methyl-butyl provides a material with mixed valence state that has conducting wires.[35]

Here, the procedure described by Danila was reproduced in order to obtain coiled fibers of C_3-TTF.[31] Then, the resulting helical fibers were doped with iodine (I_2) vapors to reach the mixed valence state material comprising TTF^0 and $TTF^{+\bullet}$ (dC_3-TTF).

Before applying the new methodology on the dC_3-TTF material on a gold surface, some previous tests were performed to corroborate the comparability of the EFM with bimodal mode signals. Firstly, a reference substrate with materials of dissimilar electrical properties - silicon containing a gold strip of 100 μm of width and 50 nm of height - was tested. A first scan on the edge of the gold strip in EFM mode was performed and so, the amplitude of vibration in the second mode of resonance was recorded. Once the image was finished, the working mode of the microscope was changed to bimodal. The AC voltage used to drive the cantilever piezo at the second resonance frequency of the cantilever was adjusted, so that the value of the amplitude of vibration in bimodal mode was similar to the vibrational amplitude value in EFM mode. Moreover, the amplitude of vibration of the cantilever in the first mode and the set-point were maintained constant in both modes. The topography (**Fig. 3a**) showed a clear difference in the silicon and gold parts of the substrate due to the difference in height between them. In the image corresponding to the amplitude in the second mode acquired in EFM (**Fig. 3b**) the metallic part, corresponding to the gold, from the semiconducting region, corresponding to the silicon, could be clearly identified. However, in the amplitude image of the bimodal mode (**Fig. 3c**) almost no contrast between the two materials could be spotted, confirming in this way that the mechanical properties of both parts were similar, as expected. Control experiments in which the DC bias was changed were performed in order to ensure a true electrostatic signal acquired **(see Fig S3 in S.I.).** With all this data, it could be concluded that contrasted images acquired by EFM mode depended only on the electrostatic properties of the sample.

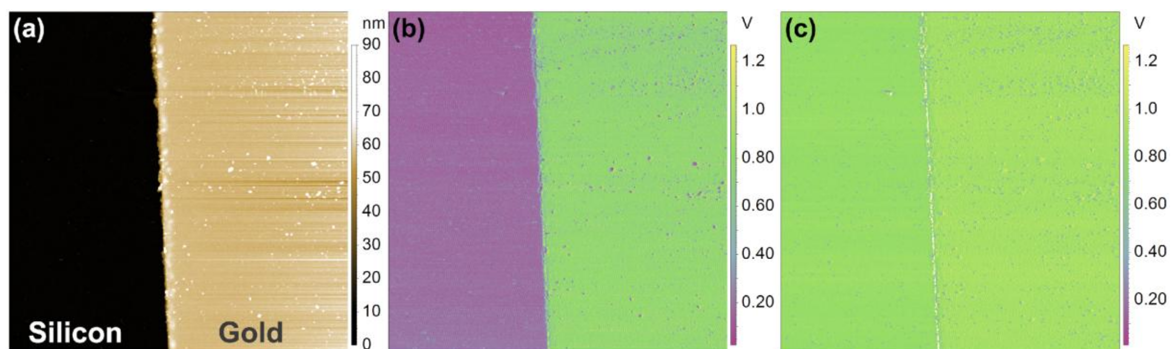

Fig 3. Images 20x20 μm of the reference substrate with gold and silicon areas. a) Topography image, b) EFM amplitude image and, c) the corresponding image of the amplitude acquired in bimodal mode. EFM images were performed by applying a tip bias of 1VAC while sample bias was fixed at -2VDC.

Additionally, other control experiment to compare the difference between working in and out of resonance in terms of signal-to-noise ratio of the electrostatic signal acquired was performed, demonstrating the dependence of the electrostatic signal with the voltage used and the amplitude of vibration of the cantilever with the AC voltage. (**Fig S3 of S.I**.).

The last control experiment using the substrate of reference was performed with the aim of demonstrating the bi-directionality of the effect of crosstalk in both modes, EFM and bimodal. In order to confirm that truly electrostatic signal was acquired, the substrate of reference was scanned, biasing the tip at 2 V in AC and working in resonance, while at the same time, the voltage in DC was sequentially changed (**Fig S4 of S.I.**).

Once the method was demonstrated using the reference sample, different regions of the dC_3-TTF sample on a gold surface were chosen with the aim to discern the electrostatic from the mechanical contributions. Each one of the selected areas was firstly scanned using EFM mode and sequentially, when the image was already obtained, the working mode was changed to

bimodal, acquiring the corresponding image for this mode in the same area. In the first area scanned (**Fig. 4a**), hardly any differences could be appreciated in the acquired images corresponding to the amplitude responses when bimodal (**Fig. 4b**) and EFM (**Fig. 4c**) modes were compared. In order to clarify whether in this case the mechanical response could be overlapped to the electrostatic, deviations in the amplitude profiles in the two modes were compared. According to the proposed method, a similar image, from the comparison of Fig. 4b and Fig. 4c, would mean that a strong mechanical coupling occurs in the EFM images. For the dC_3-TTF sample, in the fiber area, the magnitude of both bimodal and EFM amplitude images, indicates a large mechanical crosstalk. Moreover, the background of the sample showed slight differences in amplitude response, suggesting that mechanical crosstalk was less pronounced with respect to the large fibers. In order to clearly see the similarities, two profiles were extracted, a topography profile and second mode amplitude profile, Figure 4d top and bottom, respectively. As expected, both topography profiles are extremely similar, as well as tip amplitude magnitude profiles corroborating again the presence of mechanical crosstalk.

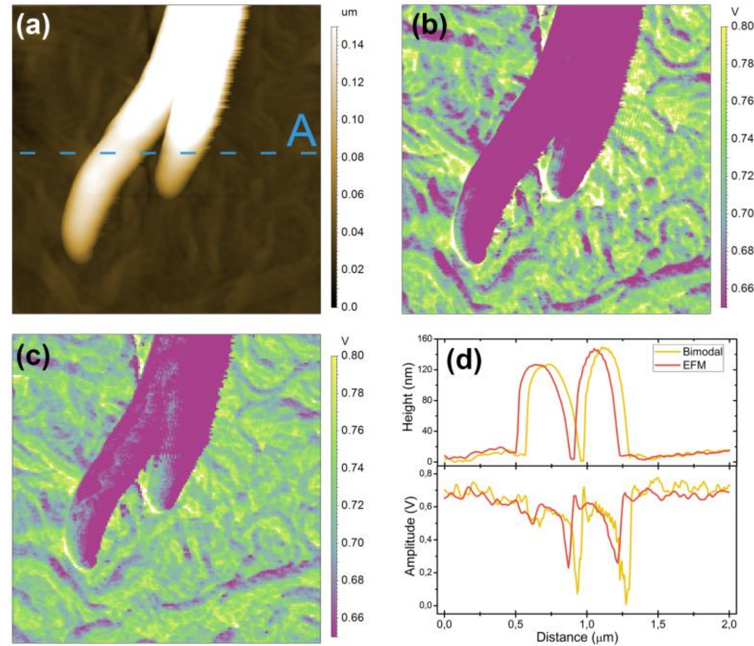

Fig. 4 Images of 2x2 μm of the dC_3-TTF sample on gold corresponding to a) topography, amplitude image of b) bimodal mode and c) EFM mode and, d) height and amplitude profiles obtained from bimodal and EFM modes. Blue-dashed line in a) indicates where the profiles depicted in d) were acquired from.

The preparation methodology followed for the dC_3-TTF sample leads to non-homogenous areas were obtained. Therefore, different regions were evaluated to study the viability of the proposed method to discriminate mechanical from electrostatic properties of a non-homogenous sample. A second area studied (**Fig. 5a**) showed notable differences in the amplitude response images when bimodal (**Fig. 5b**) and EFM (**Fig. 5c**) modes were compared. The amplitude image obtained from bimodal (**Fig. 5b**) revealed a relatively high uniformity, in terms of mechanical contributions (compared with the other analyzed areas), probably as a result of an also very homogeneous distribution of the material on the surface. When the working mode was changed to EFM (**Fig. 5c**), a locally differentiated electrostatic response was evidenced, indicating a non-homogeneous electrostatically-charged sample thus suggesting charge-transportation between

the self-assembled doped TTF units of the dC_3-TTF compound. Moreover, the differences observed in the contrast of the amplitude EFM image respect to uniformity in the bimodal mode (differences of mechanical to electrostatic contributions), confirming that there was almost no crosstalk using this methodology and real electrostatic response was recorded.

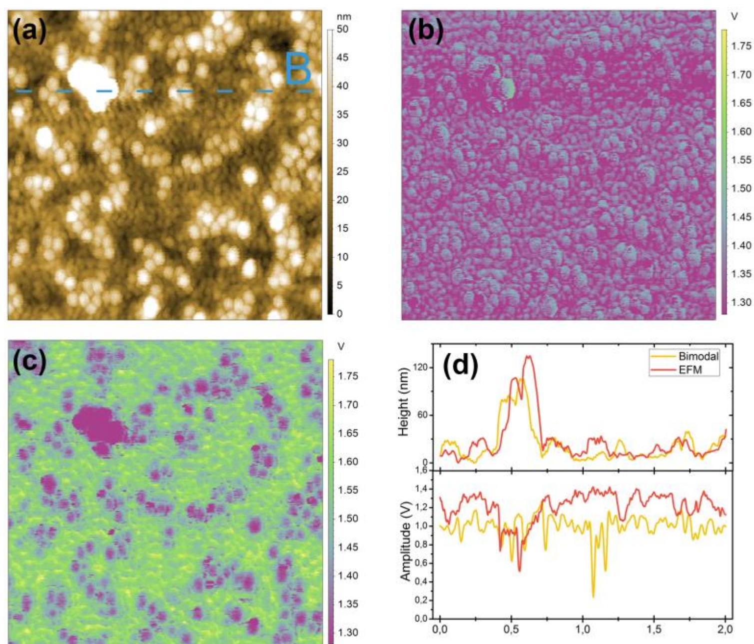

Fig. 5 Images of 2 µm x 2 µm of the dC_3-TTF sample on gold corresponding to a) topography, amplitude response of b) bimodal mode and c) EFM mode and, d) height and amplitude profiles obtained from bimodal and EFM modes. Blue-dashed line in a) indicates where the profiles depicted in d) were acquired from.

Another area was scanned which corresponded to the case where there is a mixture of mechanical and electrical responses, in comparison to the first and second area analyzed **(see Fig S5 in S.I.).** The first area analyzed has a strong mechanical interaction with the tip, while the second area analyzed has no mechanical interaction, but a huge difference in the electrostatic

interaction. This third area corresponds to the case where the sample has different mechanical and electrical properties, at the same time.

Finally in order to corroborate the bidirectionality of the effect another experiments where performed **(see Fig S6 and S7 of S.I.).**[36] With this experiment we proved that electrostatic interaction affects bimodal amplitude images. This experiment could lead to further investigations of the role of electrostatic signal in bimodal images and it is minimization.

CONCLUSIONS

A novel method based in Bimodal Atomic Force Microscopy (Bimodal) has been demonstrated to distinguish the mechanical crosstalk present in Single-pass Multifrequency Electrostatic Force Microscopy (EFM) measurements. The method has been validated after the elaboration of several calibrations and measurements of a reference sample with silicon and gold regions (with different electrostatic properties but similar mechanical characteristics). Furthermore, the crosstalk, which is always observed in EFM and in bimodal measurements of electrostatically active organic and inorganic samples with uneven mechanical properties, can be distinguished in a 'hands-on' analysis of a doped TTF-based compound with charged regions. The study has established an easy one-step methodology applicable to characterize electrostatically the surfaces of charged organic materials, with crosstalk levels far below the regular EFM and bimodal measurements, that can be easily implemented in any commercially available microscope. The observation of the pure electrostatic signal is a significant advance for determining accurately charge distribution in samples made from organic and molecular layers and materials that are used in devices derived from these materials, and may well lead to a better understanding of the nature of the surfaces of these materials and their properties.

MATERIALS AND METHODS

Materials

The reference substrate possessed a Young's modulus of 80 GPa from gold and 150 GPa for silicon. Gold surface used in the dC3-TTF analysis was a Sense bv type SPR 1.25x12.5x1 mm. C3-symmetric enantiopure tris(TTF) (N,N',N''-tris[3[3'-bis[(S)-2-methylbutylthio]-tetrathiafulvalenyl]-formylamino]-2,2'-bipyridyl]–benzene-1,3,5,-tricarboxamide) was synthesized according to the described method. C3-TTF was analysed on Sense bv type SPR 1.25x12.5x1 mm gold surfaces. The doping agent I2 (≥99.99% trace metals basis) was purchased to Sigma-Aldrich. The bimodal test sample with reference PS-LDPE-12M was purchased from Bruker Inc.

C_3-TTF sample preparation

The reference substrate composed of gold and silicon regions was cleaned by immersion in piranha solution (H_2SO_4/H_2O_2 (30%); 3:1v/v) for 10 s and rinsing thoroughly with ultrapure water. $1 \cdot 10^{-3}$ M of C_3-TTF solution in 1,4-dioxane was sonicated, heated and cooled down to room temperature, finally a drop was directly cast on a cleaned gold surface (gold surface was previously rinsed with ethanol and dried under a nitrogen stream). For doping C_3-TTF coiled fibers to obtain dC_3-TTF, the sample was exposed to I_2 vapors in a sealed container for 30 min.

Bimodal and EFM measurements

All measurements were measurements were performed in a 5500LS SPM system from Agilent Technologies with Nano World Pointprobe silicon SPM sensor tips, provided with a force constant of 2.8 N/m and Pt/Ir tip coating. The measurements were conducted under controlled atmospheric conditions by flowing compressed air to reach 6-9% of relative humidity. The Q-factor values for the electrostatically-driven and piezo-shaker-driven cantilever were calculated following Q-factor $= (|▯_{-0.7} - ▯_{+0.7}|)/▯_{▯}$, where $▯_{▯}$ corresponded to the resonance frequency of the curve, $▯_{-0.7}$ and $▯_{+0.7}$ were the values of the frequencies corresponding to $▯_{▯} \pm A \cdot 0.707$, where A is the peak amplitude. Similar amplitudes must be used in both Bimodal and EFM methods in order to compare acquired results. Because the amplitude of the electrostatically-driven cantilever depended on the tip-sample electrostatic force interactions, all variables of the EFM setup were kept constant during the experiments, using -2 V in DC and 1 V in AC, for all the scanned areas. When Bimodal measurements were conducted, the voltage applied to the piezo-shaker cantilever was changed, so the bimodal amplitude of vibration could be set identical as EFM amplitude.

ASSOCIATED CONTENT

Supporting Information

Curves of the amplitude vs. distance to quantify and calibrate the free amplitude in the first and second mode of resonance of the cantilever. Amplitude image of the reference substrate acquired by changing selectively the AC voltage and the frequency of resonance. Phase and amplitude response vs. sample bias plots in Bimodal acquired from the gold strip of the substrate of reference. Images of Bimodal and EFM modes of different area of the molecular material studied. This material is available free of charge via the Internet at http://pubs.acs.org.

AUTHOR INFORMATION

Corresponding Author

* E-mail: agomez@icmab.es

ACKNOWLEDGMENTS

MRM and AGC thank the CSIC for a JAE Predoc and a JAE-DOC grant, respectively. The work was supported by MINECO with the project MAT2013-47869-C4-2-P. AGC and AGR (ICMAB) acknowledge financial support from the Spanish Ministry of Economy and Competitiveness, through the "Severo Ochoa" Programme for Centres of Excellence in R&D (SEV-2015-0496). AGR thanks Scientific and Technical services from ICMAB.

REFERENCES

(1) Coffey, D. C.; Ginger, D. S. Time-Resolved Electrostatic Force Microscopy of Polymer Solar Cells. *Nat. Mater.* **2006**, *5*, 735–740.

(2) Girard, P. Electrostatic Force Microscopy: Principles and Some Applications to Semiconductors. *Nanotechnology* **2001**, *12*, 485–490.

(3) McFarland, F. M.; Brickson, B.; Guo, S. Layered Poly(3-Hexylthiophene) Nanowhiskers Studied by Atomic Force Microscopy and Kelvin Probe Force Microscopy. *Macromolecules* **2015**, *48*, 3049–3056.

(4) Howell, S.; Kuila, D.; Kasibhatla, B.; Kubiak, C.; Janes, D.; Reifenberger, R. Molecular Electrostatics of Conjugated Self-Assembled Monolayers on Au (111) Using Electrostatic Force Microscopy. *Langmuir* **2002**, *18*, 5120–5125.

(5) Puntambekar, K.; Dong, J.; Haugstad, G.; Frisbie, C. D. Structural and Electrostatic

Complexity at a Pentacenc/insulator Interface. *Adv. Funct. Mater.* **2006**, *16*, 879–884.

(6) Belaidi, S.; Girard, P.; Leveque, G. Electrostatic Forces Acting on the Tip in Atomic Force Microscopy: Modelization and Comparison with Analytic Expressions. *J. Appl. Phys.* **1997**, *81*, 1023–1030.

(7) Hassenkam, T.; Greve, D. R.; Bjørnholm, T. Direct Visualization of the Nanoscale Morphology of Conducting Polythiophene Monolayers Studied by Electrostatic Force Microscopy. *Adv. Mater.* **2001**, *13*, 631–634.

(8) Hong, J.; Noh, K.; Park, S.; Kwun, S.; Khim, Z. Surface Charge Density and Evolution of Domain Structure in Triglycine Sulfate Determined by Electrostatic-Force Microscopy. *Phys. Rev. B* **1998**, *58*, 5078–5084.

(9) Lei, C. H.; Das, a.; Elliott, M.; Macdonald, J. E. Conductivity of Macromolecular Networks Measured by Electrostatic Force Microscopy. *Appl. Phys. Lett.* **2003**, *83*, 482–484.

(10) Lu, Y.; Muñoz, M.; Steplecaru, C. S.; Hao, C.; Bai, M.; Garcia, N.; Schindler, K.; Esquinazi, P. Electrostatic Force Microscopy on Oriented Graphite Surfaces: Coexistence of Insulating and Conducting Behaviors. *Phys. Rev. Lett.* **2006**, *97*, 1–4.

(11) Gramse, G.; Gomila, G.; Fumagalli, L. Quantifying the Dielectric Constant of Thick Insulators by Electrostatic Force Microscopy: Effects of the Microscopic Parts of the Probe. *Nanotechnology* **2012**, *23*, 205703.

(12) Riedel, C.; Arinero, R.; Tordjeman, P.; Lévêque, G.; Schwartz, G. A.; Alegria, A.; Colmenero, J. Nanodielectric Mapping of a Model Polystyrene-Poly(vinyl Acetate) Blend by Electrostatic Force Microscopy. *Phys. Rev. E - Stat. Nonlinear, Soft Matter Phys.* **2010**, *81*.

(13) Girard, P. Electrostatic Force Microscopy: Principles and Some Applications to Semiconductors. *Nanotechnology* **2001**, *12*, 485–490.

(14) Nakamura, M.; Yamada, H. Electrostatic Force Microscopy. *Roadmap Scanning Probe*

Microsc. **2007**, 43–51.

(15) Butt, H. J.; Cappella, B.; Kappl, M. Force Measurements with the Atomic Force Microscope: Technique, Interpretation and Applications. *Surf. Sci. Rep.* **2005**, *59*, 1–152.

(16) Martin, Y.; Abraham, D. W.; Wickramasinghe, H. K. High-Resolution Capacitance Measurement and Potentiometry by Force Microscopy. *Appl. Phys. Lett.* **1988**, *52*, 1103–1105.

(17) Garcia, R.; Herruzo, E. T. The Emergence of Multifrequency Force Microscopy. *Nat. Nanotechnol.* **2012**, *7*, 217–226.

(18) Garcia, R.; Proksch, R. Nanomechanical Mapping of Soft Matter by Bimodal Force Microscopy. *Eur. Polym. J.* **2013**, *49*, 1897–1906.

(19) H. O. Jacobs, P. Leuchtmann, O. J. Homan, and a. S. Resolution and Contrast in Kelvin Probe Force Microscopy. *J. Appl. Phys.* **1998**, *84*, 6.

(20) Ziegler, D.; Rychen, J.; Naujoks, N.; Stemmer, A. Compensating Electrostatic Forces by Single-Scan Kelvin Probe Force Microscopy. *Nanotechnology* **2007**, *18*, 225505.

(21) Glatzel, T.; Sadewasser, S.; Lux-Steiner, M. C. Amplitude or Frequency Modulation-Detection in Kelvin Probe Force Microscopy. *Appl. Surf. Sci.* **2003**, *210*, 84–89.

(22) Magonov, S.; Alexander, J. Single-Pass Kelvin Force Microscopy and dC/dZ Measurements in the Intermittent Contact: Applications to Polymer Materials. *Beilstein J. Nanotechnol.* **2011**, *2*, 15–27.

(23) Stark, R. W.; Naujoks, N.; Stemmer, A. Multifrequency Electrostatic Force Microscopy in the Repulsive Regime. *Nanotechnology* **2007**, *18*, 065502.

(24) Kawai, S.; Glatzel, T.; Koch, S.; Such, B.; Baratoff, A.; Meyer, E. Systematic Achievement of Improved Atomic-Scale Contrast via Bimodal Dynamic Force Microscopy. *Phys. Rev. Lett.* **2009**, *103*, 1–4.

(25) Lozano, J. R.; Garcia, R. Theory of Multifrequency Atomic Force Microscopy. *Phys. Rev.*

Lett. **2008**, *100*, 076102.

(26) Martínez, N. F.; Lozano, J. R.; Herruzo, E. T.; Garcia, F.; Richter, C.; Sulzbach, T.; Garcia, R. Bimodal Atomic Force Microscopy Imaging of Isolated Antibodies in Air and Liquids. *Nanotechnology* **2008**, *19*, 384011.

(27) Sumali, H.; Epp, D. S. Effect of Electrostatic Force on Vibration of Micro Cantilever Beams. In; IMAC-XXIV: Conference & Exposition on Structural Dynamics, 2006.

(28) García, R. *Dynamic Atomic Force Microscopy Methods*; 2002; Vol. 47.

(29) Hutter, J. L.; Bechhoefer, J. Calibration of Atomic-Force Microscope Tips. *Rev. Sci. Instrum.* **1993**, *64*, 1868.

(30) Santos, S.; Guang, L.; Souier, T.; Gadelrab, K.; Chiesa, M.; Thomson, N. H. A Method to Provide Rapid in Situ Determination of Tip Radius in Dynamic Atomic Force Microscopy. *Rev. Sci. Instrum.* **2012**, *83*, 043707.

(31) Danila, I.; Riobé, F.; Piron, F.; Puigmartí-Luis, J.; Wallis, J. D.; Linares, M.; Ågren, H.; Beljonne, D.; Amabilino, D. B.; Avarvari, N. Hierarchical Chiral Expression from the Nano- to Mesoscale in Synthetic Supramolecular Helical Fibers of a Nonamphiphilic C 3-Symmetrical π-Functional Molecule. *J. Am. Chem. Soc.* **2011**, *133*, 8344–8353.

(32) Danila, I.; Pop, F.; Escudero, C.; Feldborg, L. N.; Puigmartí-Luis, J.; Riobé, F.; Avarvari, N.; Amabilino, D. B. Twists and Turns in the Hierarchical Self-Assembly Pathways of a Non-Amphiphilic Chiral Supramolecular Material. *Chem. Commun. (Camb).* **2012**, *48*, 4552–4554.

(33) Pop, F.; Melan, C.; Danila, I.; Linares, M.; Beljonne, D.; Amabilino, D. B.; Avarvari, N. Hierarchical Self-Assembly of Supramolecular Helical Fibres from Amphiphilic C3-Symmetrical Functional Tris(tetrathiafulvalenes). *Chem. - A Eur. J.* **2014**, *20*, 17443–17453.

(34) Canevet, D.; Sallé, M.; Zhang, G.; Zhang, D.; Zhu, D. Tetrathiafulvalene (TTF) Derivatives: Key Building-Blocks for Switchable Processes. *Chem. Commun. (Camb).*

2009, *7345*, 2245–2269.

(35) Danila, I.; Riobé, F.; Puigmartí-Luis, J.; Pérez del Pino, Á.; Wallis, J. D.; Amabilino, D. B.; Avarvari, N. Supramolecular Electroactive Organogel and Conducting Nanofibers with C3-Symmetrical Architectures. *J. Mater. Chem.* **2009**, *19*, 4495.

(36) Baumann, M.; Stark, R. W. Dual Frequency Atomic Force Microscopy on Charged Surfaces. *Ultramicroscopy* **2010**, *110*, 578–581.

SUPPORTING INFORMATION

Distinguishing Between Mechanical and Electrostatic Interaction in Single-Pass Multifrequency Electrostatic Force Microscopy on a Molecular Material

Marta Riba-Moliner,[†] *Narcis Avarvari,*[‡] *David. B. Amabilino,* [§] *Arántzazu González-Campo,*[†] *Andrés Gómez-Rodríguez*[*,†]

[†] Institut de Ciència de Materials de Barcelona (ICMAB-CSIC), Campus UAB, 08913 Bellaterra, Barcelona, Spain

[‡] Laboratoire MOLTECH-Anjou UMR 6200, UFR Sciences, CNRS, Université d'Angers, Bât. K, 2 Bd. Lavoisier, 49045 Angers, France

[§] School of Chemistry, The University of Nottingham, University Park, Nottingham NG72RD United Kingdom

S1

The free amplitude of resonance of the cantilever was taken as a reference value (2.4 V, in dynamic mode). Then, the tip was progressively approached to a pure gold surface until its free amplitude of resonance became affected due to the proximity to the surface, until both were in contact (**Fig. S1**). With the linear fitting of the region at left side of point A-see Fig. S1-a calibration constant for the amplitude signal is found, which transforms voltage units into nanometer units. With such calibration constant, we can provide a value of the specific tip-

sample distance while performing single pass EFM and Bimodal images, which was 40-60 nm. In order to acquired the EFM and Bimodal images a reduction of 25-35% of free amplitude value was used as a setpoint value. The parameters are in accordance with the literature to provide good quality sample topography images, into the repulsive regime, but without exerting to much force to the tip, so it is preserved..

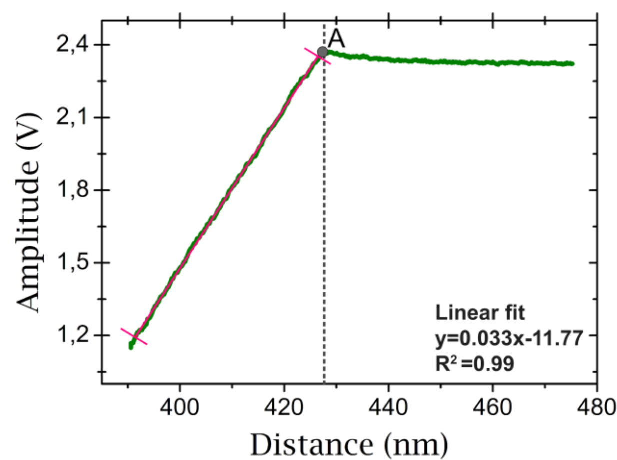

Fig. S1 Curve of the amplitude vs. distance to quantify and calibrate the free amplitude in the first mode of resonance of the cantilever. Linear fit was approached □ = □□ + □.

S2

The amplitude in the second mode of resonance had to be calibrated as well, also though the plotting of the curve amplitude *versus* the distance (**Fig. S2**). In this case, the amplitude of vibration of the cantilever was amplified with a factor of x16 to ensure a good signal-to-noise ratio. Fitting the region of the curve that comprised the interaction tip-surface zone (**Fig. S2**, below point A), the specific set-point for the second mode of vibration could be ranged between 0.2-1 nm, depending on the specific properties of the sample.

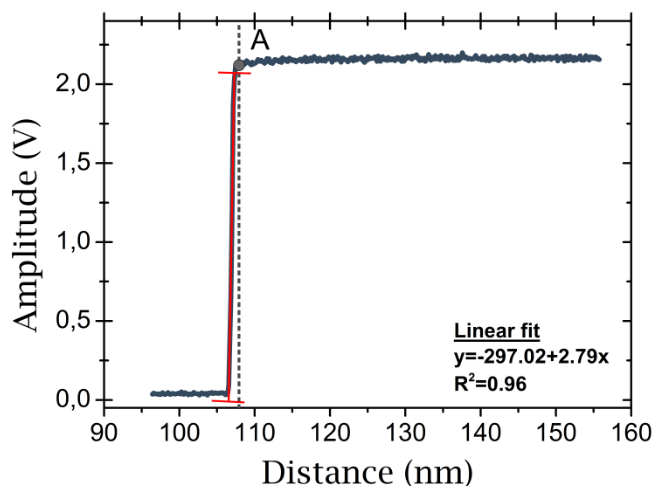

Fig. S2 Curve of the amplitude vs. distance to quantify and calibrate the free amplitude in the second mode of resonance of the cantilever. Linear fit was approached □ = □□ + □.

S3

A control experiment to compare the outgoing signal of working in resonance and out of resonance, in terms of signal-to-noise ratio, was elaborated. The reference sample was scanned in Single-pass Electrostatic Force Microscopy, at the interface between the gold and the silicon region. During the scan, the amplitude and frequency of the tip voltage was changed, as it can be seen in **Fig. S3**. This experiment also demonstrates the dependence of the electrostatic signal with the voltage used as well as with the frequency used. Working in resonance increased dramatically the electrostatic signal compared with working out of it, the signal increased by 300% (**Fig. S3a-c**). This evidence would enable a further decrease of the tip voltage, resulting in a gain of electrical lateral resolution, as the electrostatic field distribution under the tip has a circular distribution. From the profile depicted in **Fig. S3b**, the differentiation of the electrostatic response of the materials in the reference substrate could be clearly observed by using the second resonance frequency of the cantilever. The dependence of the amplitude of vibration of the cantilever with the AC voltage was also established, as expected, together with the increasing independence of the signal of the driving voltage using the second frequency of the resonance. The amplitude signal recorded for the gold part was obviously more intense due to its conductive nature.

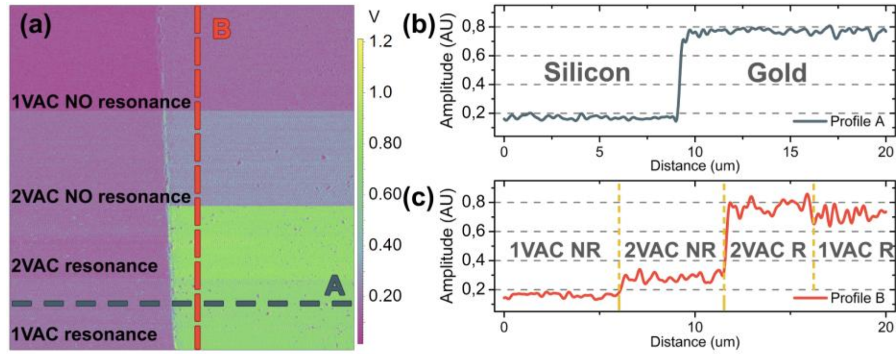

Fig. S3 a) Amplitude image of the reference substrate (20x20 µm) acquired by changing selectively the AC voltage and the frequency of resonance at 1 V and 10 kHz, 2 V and 10 kHz, 2 v and 471.58 kHz and 1 V and 471.58 kHz, from the top to the bottom. b) The amplitude vs. distance profile on the X-axis and, c) the amplitude vs. distance profile on the Y-axis. The DC voltage was kept constant during the scan at -2 V tip bias.

S4

The sensitivity of the cantilever in and out of resonance to the DC forces could be compared by extracting the slope of the curves using a linear fit, concluding that working in resonance improved the sensitivity by a factor of approximately 4.8, **Fig. S4a**. On the other hand, changing DC bias from +2, to 0 and -2 V, changed the magnitude of the amplitude image as well as shifting the electrostatic phase image by almost 180º as expected if an electrostatic signal was recorded. This change was in concordance with the fact of changing from attractive to repulsive forces when the voltage changes, so it could be concluded that electrostatic signal was acquired, Fig. S4b and S4c.

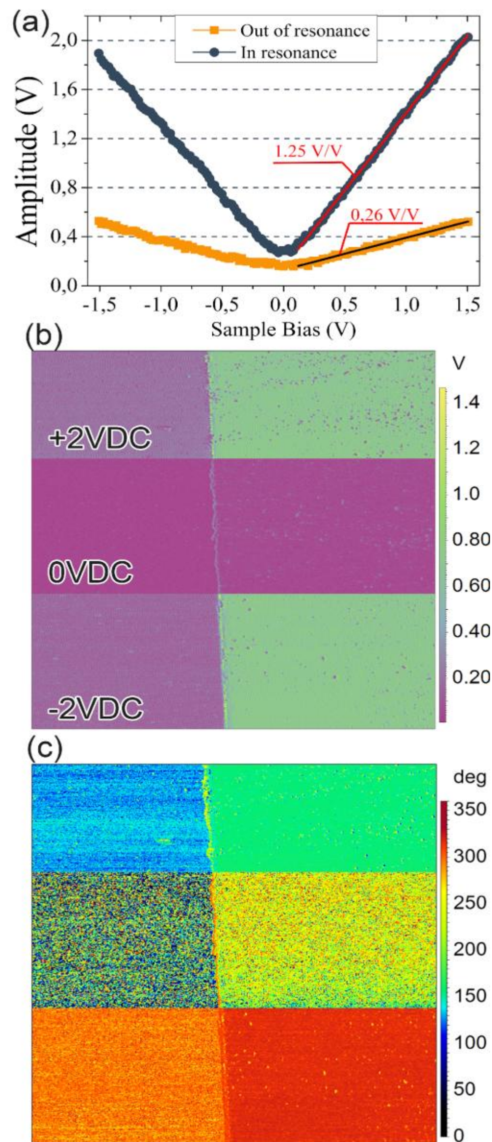

Fig. S4 a) Amplitude *vs.* sample bias obtained from a tip bias of 2 V in AC (the second frequency of resonance of the cantilever, 471.58 kHz) voltage and then changing to a DC voltage on the gold of the substrate of reference. b) Amplitude response and c) phase images of 20x20 µm from the substrate of reference acquired in EFM mode with a fixed tip bias of 2 V in AC and working in resonance.

S5

The results of another analyzed area of the sample are showed in Figure S5, where S5a is the topography of the scanned area, S5b is the bimodal amplitude image, S6c is the electrostatic amplitude image and S5d is the profile line C. In the case of the Bimodal representing the amplitude response (Fig. S5b), the main fiber core showed differentiated regions, meaning that possessed uneven mechanical properties, while in EFM amplitude image (Fig. S5c) a more uniform contrast was spotted. Amplitude profiles can be used to observe that those mentioned regions of the fiber where the ones that differed when signals were overlapped. In this situation, we can interpret the data as a mixture of mechanical and electrical response, respect to the previous area analyzed.

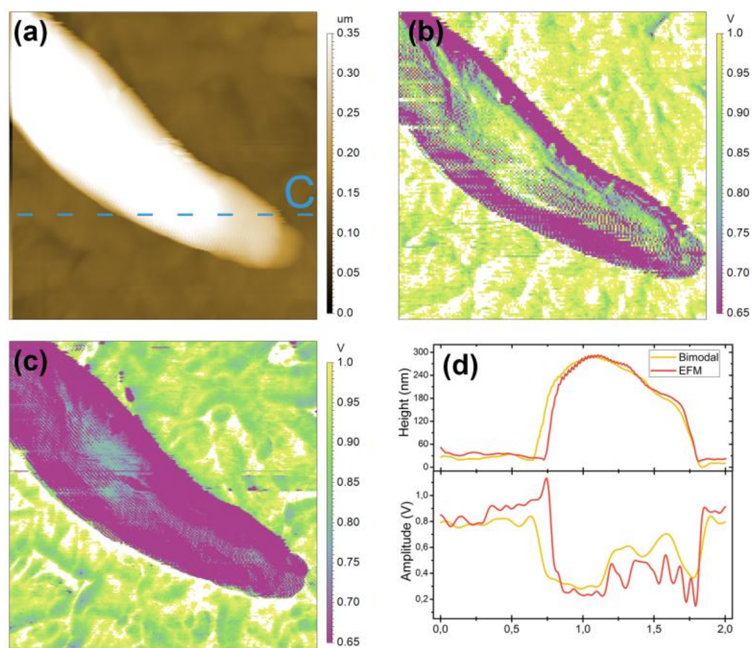

Fig. S5 Images 2x2 µm corresponding to a) topography, amplitude response of b) Bimodal mode and c) EFM mode and, d) height and amplitude profiles obtained from Bimodal and EFM modes. Blue-dashed line in a) indicates where the profiles depicted in d) were acquired from.

S6

To prove the bi-directionality of the effect, the substrate of reference was scanned using Bimodal mode. Two experiments were carried out, firstly, the tip was placed over the gold stripe and the sample bias was sequentially changed from -5 V to +5 V in DC at a 20 V/s of rate while scanning in Bimodal (**Fig. S6a**). Secondly, different voltages in DC were used to scan the substrate of reference, ranging from -2 V to +2 V in DC **(Fig. S6b)**.

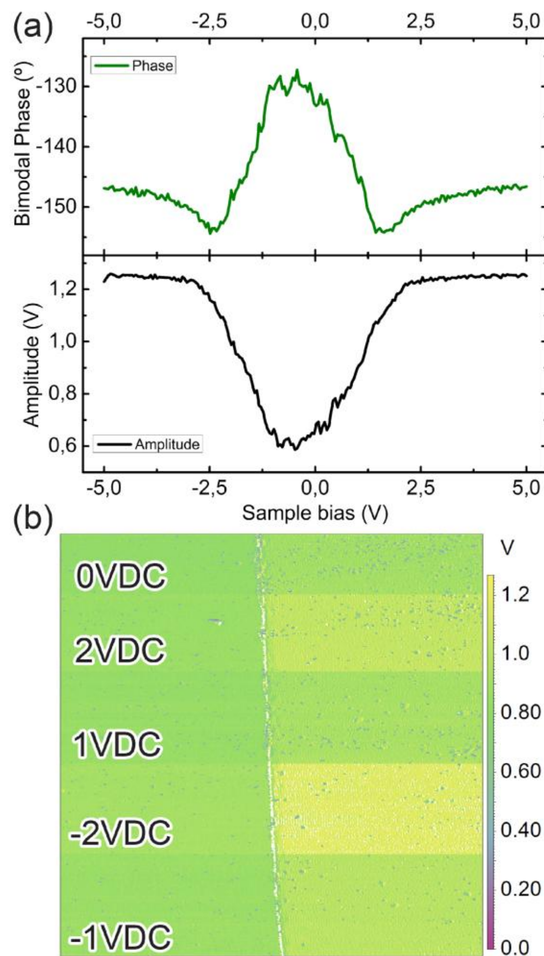

Fig. S6 a) Phase and amplitude response vs. sample bias plots in Bimodal acquired from the gold strip of the substrate of reference, the AC voltage was fixed at the second frequency of resonance

of the cantilever (471.58 kHz). b) Amplitude image 20x20 µm of the substrate of reference acquired by changing sequentially the voltage values in DC.

In order to clarify what is the contribution of Electrostatic into Bimodal image we have performed another set of experiments over a Bimodal test sample with reference number PS-LDPE-12M from Bruker company. The sample is a blend of Polystyrene (PS) and Polyolefin Elastomer(PE) with young modulus of 2GPa and 0.1GPa, respectively. The sample was scanned connected to the DC generator of the AFM, and Bimodal AFM images were performed-see Figure S7a, topography image and Figure S7b, Bimodal Amplitude image. While performing the Bimodal images, the DC bias applied to the sample was changed, from +7VDC, to 0VDC and -7VDC, as denoted by green and red lines of Fig. S7a. It can be seen that the bimodal phase image is barely affected, as we are scanning dielectric sample, there is no contribution from charge trapped inside the sample or by electrostatic interactions.

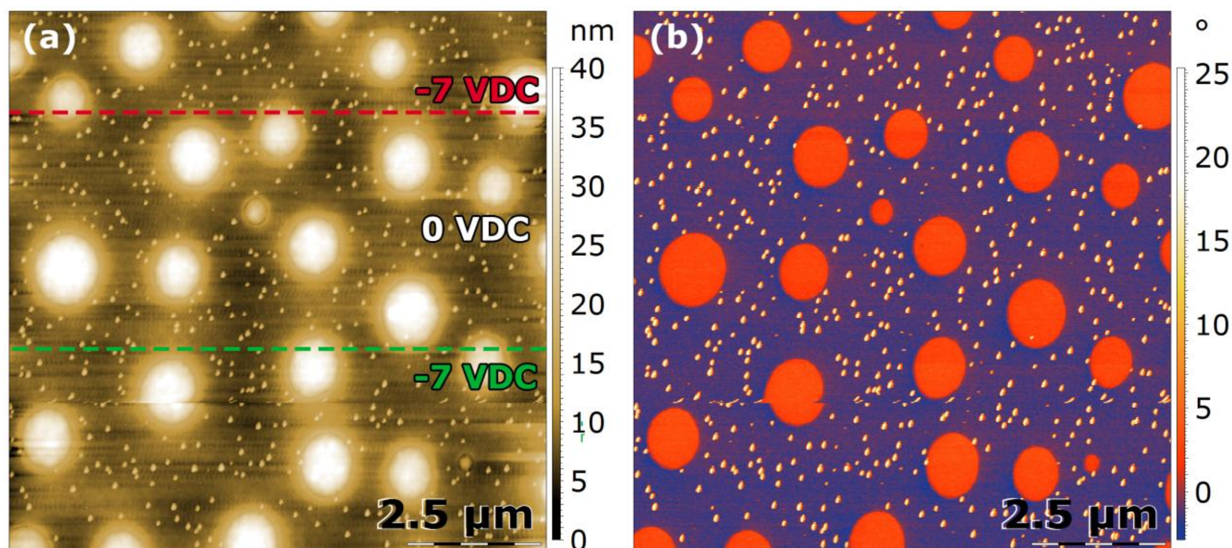

Figure S7a; Topography and **Figure S7b,** Bimodal Phase image of the proposed test sample consisting of a blend of Polystyrene (PS) and Polyolefin Elastomer(PE). Bimodal phase image

reveals the different mechanical properties in the sample, being the circles, softer PE regions, compared to the PS background. Upon different applied DC bias, there is no change in Bimodal phase confirming that the Bimodal phase image is not affected for such applied bias.